CHEMISTRY
A EUROPEAN JOURNAL

DOI: 10.1002/chem.200902611

Copper(II) Complexes of a Hexadentate Mixed-Donor N_3S_3 Macrobicyclic Cage: Facile Rearrangements and Interconversions

Craig A. Bell,[a, b] Paul V. Bernhardt,*[a] Lawrence R. Gahan,[a] Manuel Martínez,[c] Michael J. Monteiro,[a, b] Carlos Rodríguez,[c] and Clint A. Sharrad[a]

Dedicated to Professor Alan Sargeson (1930–2008), the pioneer of cage chemistry. A great leader, mentor, and friend to so many.

Abstract: The potentially hexadentate mixed-donor cage ligand 1-methyl-8-amino-3,13,16-trithia-6,10,19-triazabicyclo[6.6.6]eicosane (AMME-N_3S_3sar; sar = sarcophagine) displays variable coordination modes in a complex with copper(II). In the absence of coordinating anions, the ligand adopts a conventional hexadentate N_3S_3 binding mode in the complex [Cu(AMME-N_3S_3sar)]$(ClO_4)_2$ that is typical of cage ligands. This structure was determined by X-ray crystallography and solution spectroscopy (EPR and NIR UV/Vis). However, in the presence of bromide ions in DMSO, clean conversion to a five-coordinate bromido complex $[Cu(AMME\text{-}N_3S_3sar)Br]^+$ is observed that features a novel tetradentate (N_2S_2)-coordinated form of the cage ligand. This copper(II) complex has also been characterized by X-ray crystallography and solution spectroscopy. The mechanism of the reversible interconversion between the six- and five-coordinated copper(II) complexes has been studied and the reaction has been resolved into two steps; the rate of the first is linearly dependent on bromide ion concentration and the second is bromide independent. Electrochemistry of both $[Cu(AMME\text{-}N_3S_3sar)]^{2+}$ and $[Cu(AMME\text{-}N_3S_3sar)Br]^+$ in DMSO shows that upon reduction to the monovalent state, they share a common five-coordinated form in which the ligand is bound to copper in a tetradentate form exclusively, regardless of whether a six- or five-coordinated copper(II) complex is the precursor.

Keywords: bromine · cage compounds · copper · EPR spectroscopy · macrocycles

Introduction

The macrobicyclic hexaamine cage ligands sepulchrate (sep)[1] and sarcophagine (sar)[2] occupy a pivotal place in coordination chemistry (Scheme 1). Their most enduring feature is their proclivity for hexadentate coordination, even with metal ions not commonly associated with forming six-coordinated hexaamine complexes. Most cage chemistry has focused on the hexaamine sep and sar ligands[2] and their

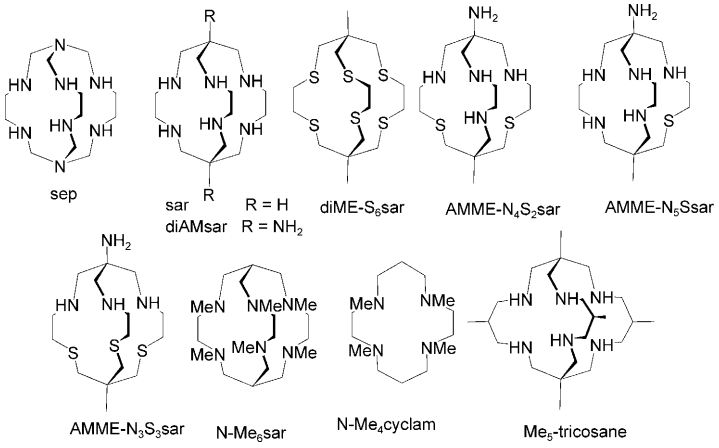

Scheme 1. Line drawings of related macrocylic ligands discussed in this paper.

[a] C. A. Bell, Prof. P. V. Bernhardt, Prof. L. R. Gahan, Prof. M. J. Monteiro, Dr. C. A. Sharrad
School of Chemistry and Molecular Biosciences
University of Queensland, Brisbane 4072 (Australia)
Fax: (+61) 7-3365-4299
E-mail: p.bernhardt@uq.edu.au

[b] C. A. Bell, Prof. M. J. Monteiro
Australian Institute for Bioengineering and Nanotechnology
University of Queensland, Brisbane 4072 (Australia)

[c] Prof. M. Martínez, C. Rodríguez
Departament de Química Inorgànica
Universitat de Barcelona, Martí i Franquès 1–11
08028 Barcelona (Spain)

Supporting information for this article is available on the WWW under http://dx.doi.org/10.1002/chem.200902611.

analogues. This is due to the ease of their synthesis by means of metal-directed chemistry of hexaamine precursors, particularly $[Co(en)_3]^{3+}$ (en = ethylenediamine), which has enabled their syntheses on large scales.

Due to inherent synthetic challenges, cages based on the sar structure but which bear donor atoms other than nitrogen are less common. The diME-S_6sar ligand (Scheme 1) is synthesized by means of a metal-free route,[3] but low yields have limited studies of its coordination chemistry beyond cobalt. Mixed-donor N/S sar ligands have been reported (Scheme 1) that comprise combinations such as (N_3S_3),[4–7] (N_4S_2),[8–11] and (N_5S)[12,13] donor atoms, accessible through Co^{III}-directed chemistry of suitably configured, preformed, mixed-donor (N/S) acyclic hexadentate ligands. Complexes of AMME-N_3S_3sar (Scheme 1) are the most extensively studied of all N/S mixed-donor cage ligands from this family, and their Co^{III},[4–6,14–16] Fe^{II},[17] and Hg^{II}[18] complexes all exhibit the expected N_3S_3 hexadentate coordination mode.

Regardless of their donor set, few examples of anything but hexadentate coordination are reported for ligands from the sar family. One such example is the hexa-N-methylated ligand N-Me_6sar (Scheme 1), for which methylation of all secondary amines generates a ligand that is unable to coordinate as a hexadentate due to steric constraints on the tertiary amine donor atoms.[19] Instead, tetradentate coordination is found when bound to Cu^{II} and Ni^{II}. This mode of binding mimics that of the obligate tetradentate tetramethylated cyclam (N-Me_4cyclam).[20–24] Indeed, the structural, spectroscopic, and electrochemical properties of the Cu^{II} and Ni^{II} complexes of N-Me_6sar and N-Me_4cyclam are essentially the same.

Although demetalation of any hexadentate sar-type complex should proceed through such partially (e.g., tetradentate) coordinated forms of the ligand, identification of these intermediates is difficult given the harsh conditions required to remove the metal from the cage. Complete removal of Co from sar-derived cages can only be achieved after reduction to the less stable and more labile Co^{II} form, followed by either complexation with cyanide or protonation of the free ligand.[25] In less constrained macromonocyclic Co^{III} complexes, equilibrium and mechanistic information has been obtained identifying both ligand substitution plus amine and thioether inversion reactions.[26,27]

The copper(II) chemistry of cage ligands is distinct from other transition metals due to its extreme lability and unusual coordination geometries. The d^9 Cu^{II} metal ion in a six-coordinate environment undergoes a spontaneous distortion from octahedral or trigonal symmetry due to the Jahn–Teller effect.[28,29] This is nearly always manifested in an elongation of a pair of *trans*-cooordinated ligands in a six-coordinate complex. Such a tetragonal distortion opposes the threefold symmetry of sar-type ligands, and indeed this lowering of symmetry has been observed and reported on a number of occasions with different cage ligands in complexes with Cu^{II}.[11,30,31]

Removal of labile divalent Cu[32] and Hg[33] from ligands that belong to the sar family is remarkably slow in comparison with the processes that occur on nonoctahedrally encapsulating polyamines,[34,35] but it is able to be observed and studied under less extreme conditions than those required for demetalation of Co cage complexes. The rate of demetalation is also dependent on the nature of the apical substituents. For instance, the complex $[Cu(diAMsar)]^{2+}$ (Scheme 1) is remarkably resistant to acid-promoted demetalation.[30,32] However, reduction to Cu^{I} or zero-valent Cu leads to immediate complex dissociation.[36] Indeed, only the expanded-cavity hexaamine cage complex $[Cu(Me_5\text{-tricosane})]^{2+}$ (Scheme 1) exhibits quasireversible $Cu^{II/I}$ electrochemistry and makes it unique among the copper cage complexes in this respect.[31]

Great interest in understanding the Cu chemistry of polyamines stems from their extensive use as catalysts in "living" radical polymerization.[37–40] The Cu^{II} complex of the mixed donor ligand AMME-N_3S_3sar has been of interest recently with respect to its activity as a catalyst to significantly enhance the coupling reaction between α,ω-polystyrene (Br-PSTY-Br) to make multiblock copolymers in organic solvents, particularly DMSO.[41] A requirement in this chemistry is that the copper complex undergoes reversible $Cu^{II/I}$ electron-transfer reactions coupled with bromine-atom transfer according to Equation (1). Alkyl chlorides and iodides are also known to participate in this chemistry.[42]

$$LCu^{I} + RBr \rightleftharpoons LCu^{II}Br + R^{\bullet} \quad (1)$$

The activation step involves partial oxidative addition of an alkyl bromide, in this case to a Cu^{I} complex that generates a Cu^{II}–bromido complex, thus liberating a radical that then participates in the polymerization reaction. The reverse (deactivation) reaction is also important in providing kinetic control over the polymerization reaction.

The poor deactivating capability of radicals by the Cu^{II} complex of AMME-N_3S_3sar led us to undertake a comprehensive study of its solution properties in the presence and absence of bromide. Herein we report some remarkably facile and unexpected reactions between different structural forms of the complex that have a significant bearing on its application in metal-catalyzed "living" radical polymerization.

Results and Discussion

Synthesis and structural characterization: Complexation of AMME-N_3S_3sar with Cu^{II} is rapid and straightforward, but the final product isolated from the reaction is strongly dependent on the choice of Cu salt. When copper(II) bromide is chosen, dark blue-green needles of a copper complex are obtained. The X-ray crystal structure of this complex $[Cu(AMME\text{-}N_3S_3sar)Br]Br\cdot 3H_2O$ reveals the cage ligand to be bound to Cu in a tetradentate N_2S_2 manner (Figure 1). All other crystal structures of AMME-N_3S_3sar complexes to

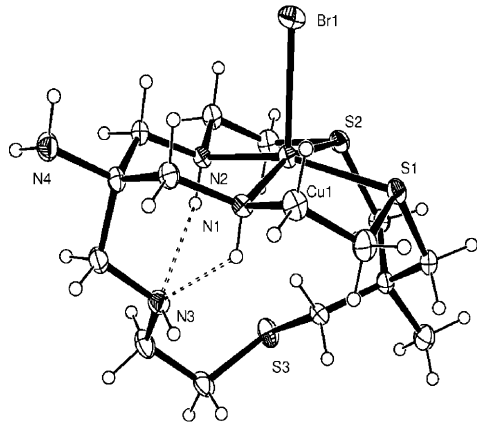

Figure 1. ORTEP plot of the $[Cu(AMME\text{-}N_3S_3sar)Br]^+$ cation (30% probability ellipsoids shown). Selected distances [Å] and angles [°]: Cu–N1 2.025(2), Cu–N2 1.998(3), Cu–S1 2.312(1), Cu–S2 2.330(1), Cu–Br1 2.5548(7); N2-Cu-N 193.3(1); N2-Cu-S1 162.44(7), N1-Cu-S1 87.54(8), N2-Cu-S2 87.07(7), N1-Cu-S2 162.69(7), S1-Cu-S2 87.02(4), N2-Cu-Br1 100.44(7), N1-Cu-Br1 99.66(6), S1-Cu-Br1 96.70(3), S2-Cu-Br1 97.29(2). Hydrogen bonds are shown with dashed lines.

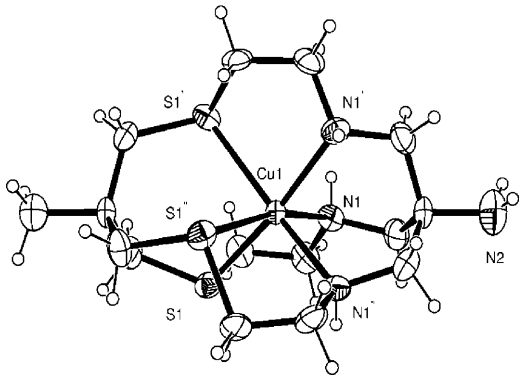

Figure 2. ORTEP plot of the $[Cu(AMME\text{-}N_3S_3sar)]^{2+}$ cation (30% probability ellipsoids shown). Selected distances [Å] and angles [°]: Cu1–N1 2.114(5), Cu1–S1 2.471(2); N1-Cu1-S1′ 83.0(2), N1-Cu1-S1 167.1(2), N1-Cu1-S1′ 100.9(2), N1-Cu1-N1′ 89.7(2), S1-Cu1-S1″ 87.93(6). Primes and double primes denote symmetry operations: $z-1/2$, $-x+3/2$, $-y+2$ (′) and $-y+3/2$, $-z+2$, $x+1/2$ (″).

date (including substituted analogues) have revealed a hexadentate binding mode.[4,7,16,17]

An axially coordinated bromido ligand completes the square-pyramidal coordination sphere, whereas the other bromide ion is not coordinated. Three water molecules complete the asymmetric unit of the structure. The Cu ion is displaced approximately 0.32 Å above the N_2S_2 plane toward the Br^- ligand. The S-donor lone pairs and the coordinated secondary amine hydrogen atoms are on opposite sides of the N_2S_2 plane in the so-called *trans*-III configuration originally defined for cyclam complexes.[43] The coordinated secondary amines donate intramolecular hydrogen bonds to the uncoordinated secondary amine (N3), and this feature appears to be important in stabilizing the structure. An additional unusual feature of note is an agostic Cu···H bond (2.32 Å) that involves a methylene proton adjacent to the uncoordinated S atom. By comparison, the hexamethylated N-Me_6sar ligand when bound to Cu^{II} finds all four N-methyl groups on the same side of the N_4 plane (the *trans*-I configuration). The Cu–N and Cu–S coordinate bonds are typical of those found in structurally related macrocyclic Cu^{II} complexes.[44,45]

Complexation of AMME-N_3S_3sar with $Cu(ClO_4)_2{\cdot}6H_2O$ (lacking a competitive coordinating anion) leads to a distinctly different complex in which the Cu ion is completely encapsulated by the ligand. The crystal structure of $[Cu(AMME\text{-}N_3S_3sar)](ClO_4)_2$ was determined and hexadentate coordination of the cage ligand is apparent (Figure 2). The complex cation occupies a crystallographic threefold rotation axis (oriented horizontally as drawn in Figure 2), which includes the Cu atom and the apical exocyclic primary amine (N2). The perchlorate anions are disordered about threefold axes and are not shown in Figure 2.

The trigonal symmetry of the Cu complex is only apparent, as the cation is actually disordered about this threefold axis and its true tetragonally elongated coordination geometry is only resolved by spectroscopy (see below). No truly octahedral or threefold (trigonally) symmetric Cu^{II} complexes are known. The Jahn–Teller effect[46] always overrides any ligand field effects, thus resulting in a spontaneous distortion (usually an elongation) of one pair of *trans*-disposed ligands, thus removing the degeneracy of the ^2E ground electronic state in an octahedral or trigonal ligand field.

The present case of apparent symmetry is not unusual. There are a number of other cases in which low-symmetry hexaamine Cu^{II} complexes crystallize on (impossibly) high symmetry sites (trigonal or hexagonal)[30,47] or, when appearing on general sites, exhibit anomalous coordination geometries such as pseudooctahedral[48] or tetragonally compressed.[31] Regardless of the "apparent" structure obtained in the solid state, they all have been found in solution to exhibit tetragonally elongated (4+2) coordination geometries. The structure of $[Cu(AMME\text{-}N_3S_3sar)](ClO_4)_2$ is yet another example of this type of behavior.

Bearing this in mind, the observed Cu–N and Cu–S bond lengths in $[Cu(AMME\text{-}N_3S_3sar)](ClO_4)_2$ are only a weighted average of two short bonds and one long bond. No phase change was found for this compound between 100 and 293 K, so the true molecular coordinate bonds are not known. The apparent trigonal twist angle in the structure of $[Cu(AMME\text{-}N_3S_3sar)](ClO_4)_2$ is 44° (0° for trigonal prismatic and 60° for trigonal antiprismatic). This is significantly different to the trigonally (and tetragonally) distorted $Cu^{II}N_6$ cage complexes such as $[Cu(H_2diAMsar)](NO_3)_4$ (ca. 29° twist angle) and indicates that the AMME-N_3S_3sar ligand has a distinct preference for less twisted coordination geometries. This may be due to the larger van der Waals radius of the S atom and its 1–3 nonbonded repulsion of the opposing N-donor atoms. Distinctly different threefold symmetric conformational minima have been identified in the corresponding sar cages;[49] most relevant are the so-called D_3lel_3 (pseudo-octahedral, twist angle ca. 50°) and D_3lel_3' conformers (trigonally distorted, twist angle ca. 29°).

The apical amine (bearing only two hydrogen atoms) is also disordered. Interestingly this primary amine neither donates nor accepts hydrogen bonds. All hydrogen bonds are donated by the coordinated amine (N1) and accepted by the disordered perchlorate (Cl2, O3–O6). This anion occupies a threefold axis. All attached O atoms occupy general sites, so the anion, like the complex cation, is also disordered about the threefold axis. This perchlorate is wedged between adjacent $[Cu(AMME\text{-}N_3S_3sar)]^{2+}$ cations and forms hydrogen bonds of different strengths with each. The rotational disorder of this ClO_4^- anion is clearly tied to disorder of the Cu complex cation, as movement of N1 (the only active hydrogen-bond donor in the structure) towards or away from the Cu center must affect the positions of atoms O3···O6 attached to Cl2. The amplitude of variation in Cu–N coordinate bonds (or so-called Jahn–Teller radius) from strong equatorially coordinated amines (ca. 2.0 Å, as seen in $[Cu(AMME\text{-}N_3S_3sar)Br]^+$) to weak, axially coordinated amines is typically in the range 0.3–0.4 Å in comparison with the structures of truly tetragonally elongated Cu^{II} complexes.[48,50,51] It is apparent that there is a similar variation in the hydrogen-bonding contacts between N1 and its various disordered O-atom acceptors (N1–H1···O 2.29–2.65 Å), which illustrates how the lattice can absorb local distortions of the Cu centers by reorientation of the perchlorate anions, thus preserving hydrogen-bonding interactions and also maintaining the high-symmetry cubic lattice. The structure as such is consistent with a static disorder model.

EPR spectroscopy: The true tetragonally elongated symmetry of the Cu ion in $[Cu(AMME\text{-}N_3S_3sar)](ClO_4)_2$ is revealed by EPR and UV/Vis spectroscopy. The degeneracy of the $d_{x^2-y^2}$ and d_{z^2} orbitals in either an octahedral or trigonal ligand field is removed by a tetragonal distortion of a pair of *trans*-disposed ligands. All EPR spectra were measured for frozen sample solutions in 2 mM DMSO at 140 K. Anisotropic spin Hamiltonian parameters ($g_{x,y,z}$ and $A_{x,y,z}$) are given in the Experimental Section and these were determined by spectral simulation.[52] The experimental and calculated spectra are presented in the Supporting Information.

The EPR spectrum of $[Cu(AMME\text{-}N_3S_3sar)](ClO_4)_2$ is shown in Figure 3A. The spin Hamiltonian parameters $g_z = 2.163$ ($A_z = 160$ G), $g_y = 2.076$ ($A_y = 50$ G), and $g_x = 2.038$ ($A_x = 35$ G) are consistent with that of a tetragonally elongated complex with an additional rhombic distortion ($g_z \gg g_y > g_x$ and $A_z \gg A_y > A_x$).[46] The spectrum is comparable to other Cu^{II}–polyamine complexes in six-coordinate environments including $[Cu(diAMsar)]^{2+}$ and $[Cu(AMME\text{-}N_4S_2sar)]^{2+}$, which each exhibit a tetragonally elongated structure in both the solid state and in solution.[11] These spectral features are indicative of a Cu complex with a $d_{x^2-y^2}$ ground state.[46] A notable feature is the magnitude of the largest hyperfine coupling constant A_z (160 G), which is considerably greater than that seen in the EPR spectrum of $[Cu(diAMsar)]^{2+}$ ($A_z = 130$ G), a more trigonally twisted complex (29°) as noted above. Similarly, g_z is 2.163 for $[Cu(AMME\text{-}N_3S_3sar)]^{2+}$ compared with 2.22 for $[Cu(diAMsar)]^{2+}$, which is also related to the more regular (less trigonally twisted) coordination geometry of the mixed-donor $[Cu(AMME\text{-}N_3S_3sar)]^{2+}$ complex.[30]

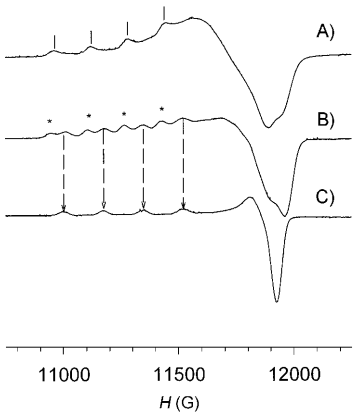

Figure 3. Q-band (33.94 GHz) EPR spectra of 2 mM frozen solutions (in DMSO; 140 K) of A) $[Cu(AMME\text{-}N_3S_3sar)](ClO_4)_2$, B) $[Cu(AMME\text{-}N_3S_3sar)](ClO_4)_2$ in the presence of 100 mM Et_4NBr (in DMSO) immediately after dissolution (ca. 2 min), and C) $[Cu(AMME\text{-}N_3S_3sar)](ClO_4)_2$ in the presence of 100 mM Et_4NBr (in DMSO) after 3 h at room temperature. The peaks highlighted by | and * symbols are due to distinctly different species.

Upon addition of 100 mM bromide ions to $[Cu(AMME\text{-}N_3S_3sar)](ClO_4)_2$ in DMSO, two species are formed within the 2 min interval required to mix the reagents and freeze the solution for measurement (Figure 3B). Upon standing at room temperature for 3 h the EPR spectrum of the same $[Cu(AMME\text{-}N_3S_3sar)](ClO_4)_2$/100 mM bromide solution simplifies to that of a single species (Figure 3C); $g_z = 2.154$ ($A_z = 164$ G), $g_y = g_x = 2.040$ ($A_y = A_x = 25$ G). All of the features of the final spectrum (Figure 3C) are apparent in the spectrum of the intermediate mixture (vertical arrows to Figure 3B), but the other component of this mixture (marked with * symbols, $g_z = 2.166$ and $A_z = 162$ G) does not correspond to that of $[Cu(AMME\text{-}N_3S_3sar)]^{2+}$ (Figure 3A, marked with | symbols, $g_z = 2.163$ and $A_z = 160$ G). Although the differences in the low-field region appear small at face value, they are significant; the uncertainties of the g_z values are less than 0.001 and the A_z values less than 1 G. Note that no significant differences can be defined in the g_x and g_y region to higher field (11 500–12 000 G) in which the much smaller hyperfine coupling constants (A_x and A_y) lead to a broad unresolved envelope of transitions.

The EPR spectrum of a freshly prepared solution of $[Cu(AMME\text{-}N_3S_3sar)Br]Br$ (Figure 4A) is typical of an axially elongated Cu^{II} complex. There are several differences from the EPR spectrum of six-coordinate $[Cu(AMME\text{-}N_3S_3sar)]^{2+}$. Firstly, g_z shifts to 2.154 (compared with 2.163 for the completely encapsulated six-coordinate complex). The peaks at higher field sharpen to a single feature, thereby indicating equivalence of the g_x and g_y transitions, that is, axial symmetry ($g_x = g_y$ and $A_x = A_y$). Upon standing at room temperature for 3 h, the EPR spectrum of $[Cu(AMME\text{-}$

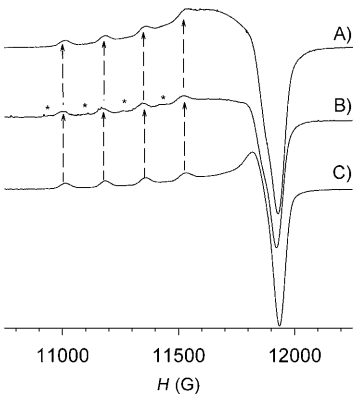

Figure 4. A) Q-band (≈33 GHz) EPR spectra of 2 mM frozen solutions (in DMSO; 140 K) of freshly prepared [Cu(AMME-N_3S_3sar)Br]Br, B) [Cu(AMME-N_3S_3sar)Br]Br after 3 h, and C) [Cu(AMME-N_3S_3sar)Br]Br in the presence of 100 mM Et_4NBr (in DMSO). The arrows show corresponding peaks between the three samples. The * symbols indicate emerging peaks in spectrum B that correspond to the starred peaks in Figure 3B.

N_3S_3sar)Br]Br evolves into that of two species (Figure 4B); one is the starting material (the dominant form in Figure 4B) and the other matches that of the intermediate marked with asterisks in Figure 3B ($g_z = 2.166$ and $A_z =$ 162 G). If the EPR spectrum of [Cu(AMME-N_3S_3sar)Br]Br is measured in the presence of 100 mM Et_4NBr in DMSO (Figure 4C: $g_z = 2.154$ and $A_z = 164$ G), a single species is observed that is essentially the same as that of a freshly prepared solution in Figure 4A (vertical arrows) and does not change significantly over time.

In summary, three species have been identified by EPR spectroscopy: the two crystallographically characterized complexes $[Cu(AMME\text{-}N_3S_3sar)]^{2+}$ (Figure 3A) and $[Cu(AMME\text{-}N_3S_3sar)Br]^{+}$ (Figures 3C, 4A, and 4C), plus an intermediate common to both reactions (highlighted in the parallel region with asterisks in Figures 3B and 4B).

Optical spectroscopy: The electronic absorption spectrum of $[Cu(AMME\text{-}N_3S_3sar)]^{2+}$ in DMSO exhibits four maxima. The two weakest bands appear at 1292 and 622 nm and are both of d–d origin (Figure S3 in the Supporting Information). The Jahn–Teller tetragonal distortion in $[Cu(AMME\text{-}N_3S_3sar)]^{2+}$ results in a large splitting of the $d_{x^2-y^2}$ and d_{z^2} orbitals (otherwise degenerate in an octahedral or trigonal ligand field).[28,30,46] The lowest-energy electronic transition (1292 nm) is between these orbitals ($d_{z^2} \rightarrow d_{x^2-y^2}$), whereas the broad visible maximum at 622 nm corresponds to three overlapping transitions from the nonbonding d_{xy}, d_{yz}, and d_{xz} orbitals of similar energy to the singly occupied $d_{x^2-y^2}$ orbital. The d–d electronic spectrum of $[Cu(AMME\text{-}N_3S_3sar)Br]^{+}$ is much simpler and only a single visible maximum (641 nm) is observed as expected for an axially elongated square-pyramidal complex in which the energy of the d_{z^2} orbital approaches that of the nonbonding d_{xy}, d_{yz}, and d_{xz} group and transitions to $d_{x^2-y^2}$ occur at about the same energy.

There are greater differences between the near-UV spectra of the two complexes in which the six-coordinate complex $[Cu(AMME\text{-}N_3S_3sar)]^{2+}$ bears two prominent $S \rightarrow Cu^{II}$ charge-transfer electronic transitions at 311 and 367 nm that merge to a single maximum at 335 nm for the five-coordinate [Cu(AMME-N_3S_3sar)Br]Br complex. To ensure that the spectrum of the latter bromido complex was obtained, the spectral solution of the complex contained a 40-fold excess of bromide ions and no significant change in the spectrum was observed over the timescale of minutes required to measure the spectrum.

By comparison, the related six-coordinate (N_4S_2) complex $[Cu(AMME\text{-}N_4S_2sar)]^{2+}$ (Scheme 1) exhibits two maxima at 330 nm ($\varepsilon = 3800\,M^{-1}cm^{-1}$) and 272 nm ($\varepsilon = 4000\,M^{-1}cm^{-1}$). The presence of two as opposed to one $S \rightarrow Cu$ ligand-to-metal charge-transfer (LMCT) transition is consistent with different Cu–S coordinate bonds (strong and weak) identified crystallographically.[11] By contrast, the five-coordinated complex $[Cu(AMME\text{-}N_3S_3sar)Br]^{+}$ shows a single $S \rightarrow Cu$ LMCT transition consistent with equivalent equatorially coordinated S donors.

Kinetics of rearrangement between [Cu(AMME-N_3S_3sar)]-$(ClO_4)_2$ and [Cu(AMME-N_3S_3sar)Br]Br: The EPR spectral changes observed for $[Cu(AMME\text{-}N_3S_3sar)]^{2+}$ in reaction with bromide ions are more accurately monitored by time-resolved electronic spectroscopy. In the presence of bromide ions (in DMSO), the electronic maxima of $[Cu(AMME\text{-}N_3S_3sar)]^{2+}$ undergo several changes on rather different timescales. The first quantifiable change in the spectrum after mixing is associated with a small growth in absorbance at 350 and 750 nm over a timescale of about 2 min (Figure 5A) with the rest of the spectrum being relatively constant during this time. The second phase of the reaction (Figure 5B) is much slower and clean isosbestic points[1] are observed that lead to complete transformation of the two UV maxima of the six-coordinate $[Cu(AMME\text{-}N_3S_3sar]^{2+}$ complex to a single peak with concomitant growth in intensity of the d--d band in the 620–640 nm range. The final spectrum is identical to that of [Cu(AMME-N_3S_3sar)Br]Br.

By varying the concentrations of copper complex and bromide (as nBu$_4$PBr) in DMSO and also the timescale and frequency of spectra data acquisition, the overall reaction could be resolved into two first-order steps (see the Experimental Section) that exhibited different rates and dependencies on bromide concentration. The initial rapid step (Figure 5A) is linearly dependent on bromide concentration (Figure S4 in the Supporting Information) with a nonzero intercept, which demonstrates that an equilibrium that involves bromide ions is established. The ratio of the forward (slope of second-order plot of k_{obs} versus bromide concentration) and back reactions (intercept of plot) gives an equilibrium constant for this initial bromide reaction of about 5. The slower reaction that follows ($k_{obs} = 2.5 \times 10^{-4}\,s^{-1}$) is inde-

[1] The position of these isosbestic points was dependent on the copper/bromide concentration ratio, thereby indicating the establishment of an equilibrium reaction for the initial reaction observed.

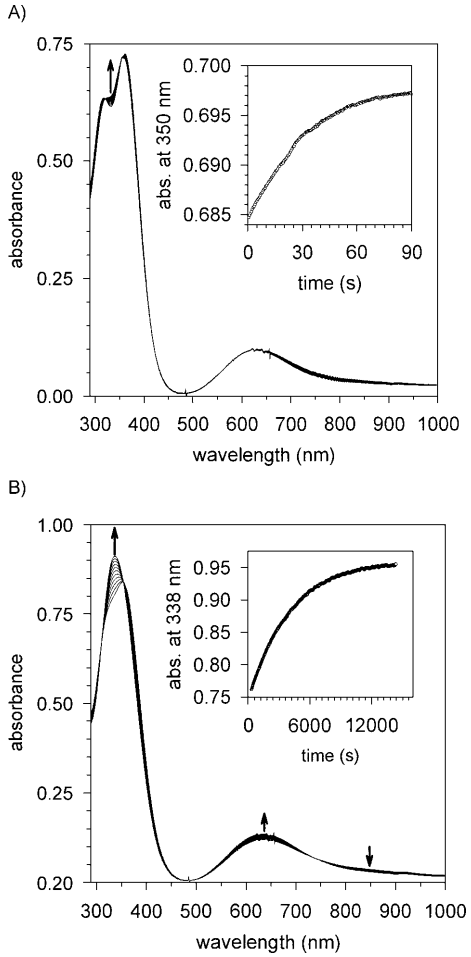

Figure 5. A) Absorption spectra shown at 5 s intervals for [Cu(AMME-N_3S_3sar)]$^{2+}$ (0.2 mM) in DMSO over the course of the first 90 s after mixing with 12.5 mM nBu$_4$PBr in DMSO; inset displays the absorbance change at 350 nm as a function of time (0.5 s intervals) and data fit to a single exponential with $k_{obs}=(2.7\pm0.2)\times10^{-2}$ s. B) Absorption spectra shown at 45 s intervals for [Cu(AMME-N_3S_3sar)]$^{2+}$ (0.2 mM) in DMSO over the course of the first 30 min of reaction with 50 mM nBu$_4$PBr in DMSO. Inset: absorbance at 335 nm as a function of time (15 s intervals) and data fit to a single exponential with $k_{obs}=(2.5\pm0.2)\times10^{-4}$ s. Minor ticks on horizontal axis correspond to 10 min intervals.

pendent of bromide concentration and implies a rearrangement of the intermediate bromido complex that generates the crystallographically characterized complex [Cu(AMME-N_3S_3sar)Br]$^+$. The intermediate species observed by EPR spectroscopy (indicated by asterisks) in Figures 3B and 4B is most likely the same complex that rearranges in the bromide-independent slow step in Figure 5B to the final crystallographically characterized complex [Cu(AMME-N_3S_3sar)Br]$^+$.

The timescales of the two processes resolved in Figure 5A and B are too long to be simple ligand-substitution reactions on copper(II).[53] In macrocyclic ligand complexes, inversion of coordinated secondary amines and S-donor lone pairs is slow and restricted by the ring system,[26,54] and conversion of [Cu(AMME-N_3S_3sar]$^{2+}$ (six-coordinate) to [Cu(AMME-N_3S_3sar)Br]$^+$ (five-coordinate) requires inversion of one coordinated N donor as well as one S donor on the same "strap" of the ligand. The two processes resolved here, on quite different timescales, are probably these same two donor-atom inversion reactions. As indicated, other events such as bromide coordination to copper should be rapid and not rate-limiting.

The time-monitored electronic spectral changes of the reverse reaction that occurs upon dissolution of [Cu(AMME-N_3S_3sar)Br]Br in DMSO (without additional bromide ions) reveal a gradual decrease in intensity of the initial 636 nm maximum (Figure 6A) and shift to shorter wavelength, whereas the UV maximum of the precursor splits into two. The final spectrum is reminiscent of (but not identical to) the six-coordinate complex [Cu(AMME-N_3S_3sar)]$^{2+}$. On the basis of the EPR spectroscopy results in Figure 5B (under similar conditions), it is likely that the observed electronic spectrum at the end of the reaction in Figure 6A is that of a mixture of complexes. In the absence of additional bromide ions, the first-order rate constants for this process varied in a complicated way: they increased with lower concentrations of both copper and bromide.

If the same dissociation reaction is monitored with a 20-fold (or more) excess of bromide in DMSO, the spectral changes become much simpler and the maxima at 335 and 636 nm are merely lowered in intensity without splitting of the UV bands as seen in Figure 6A. Under these conditions, the excess bromide ions seem to suppress any formation of the six-coordinate complex. The observed rate constant in the presence of an excess of bromide ions (Figure 6B) is the same regardless of bromide concentration ($(3.3\pm0.2)\times10^{-4}$ s^{-1}) and compares well to that obtained for the second phase of the reaction between [Cu(AMME-N_3S_3sar)]$^{2+}$ and bromide ions. This value is significantly slower than the reaction without additional bromide present. It appears that a side reaction of [Cu(AMME-N_3S_3sar)Br]$^+$ becomes important (and increases the overall rate) when bromide ions concentrations are low, thereby leading to a complex mixture of products but the exact composition of this mixture remains unknown at this time.[2]

The findings from this kinetic study are summarized in Scheme 2. The six-coordinate [Cu(AMME-N_3S_3sar)]$^{2+}$ complex may be converted to the five-coordinate [Cu(AMME-N_3S_3sar)Br]$^+$ cleanly in the presence of a large excess of bromide ions. The progress of the "reverse" dissociation reaction of [Cu(AMME-N_3S_3sar)Br]$^+$ is dependent on bromide ion concentration, and at low bromide concentrations the reaction becomes diverted and an unknown "dead end" complex is formed (in addition to [Cu(AMME-N_3S_3sar)Br]$^+$ and [Cu(AMME-N_3S_3sar)]$^{2+}$). In the presence of excess bromide ions, the dissociation of [Cu(AMME-N_3S_3sar)Br]$^+$ is more controlled, but the reaction does not go further than

[2] In this respect, it is to be noted that the monitoring of the [Cu(AMME-N_3S_3sar)]$^{2+}$ plus Br$^-$ reaction when the bromide concentration is only in a small excess (8- to 15-fold) over the copper leads to a similarly anomalous rate enhancement to that found here for the reverse reaction when bromide concentrations are low.

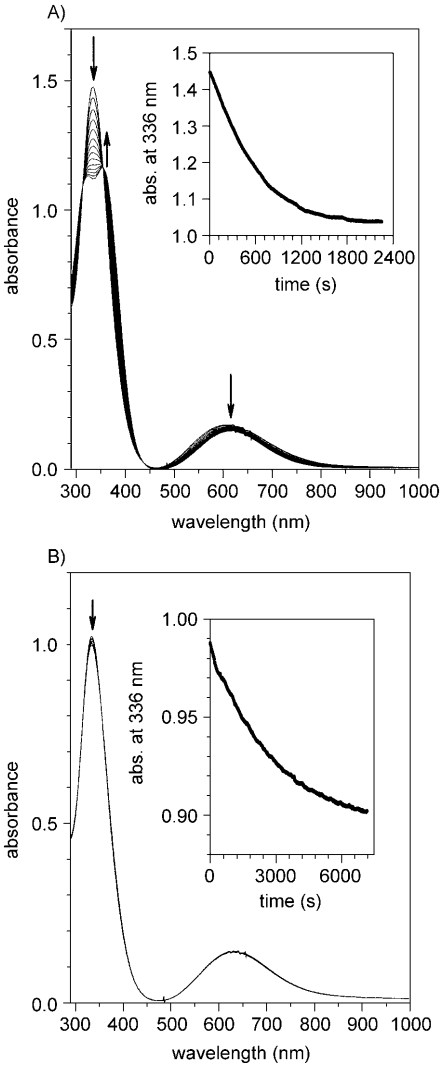

Figure 6. A) Absorption spectra shown at 90 s intervals for [Cu(AMME-N_3S_3sar)Br]Br (0.28 mM) in DMSO (no added bromide) over the course of the first 40 min of reaction. Inset: absorbance at 336 nm as a function of time (9 s intervals) and data fit to a single exponential with an apparent rate constant $k_{obs} = (1.7 \pm 0.1) \times 10^{-3}\ s^{-1}$. Minor ticks on horizontal axis are at 2 min intervals. B) Absorption spectra shown at 90 s intervals for [Cu(AMME-N_3S_3sar)Br]Br (0.37 mM) and 3 mM nBu$_4$PBr in DMSO over the course of the first 40 min of reaction. Inset: absorbance at 336 nm as a function of time (9 s intervals) and data fit to a single exponential with $k_{obs} = (3.4 \pm 0.1) \times 10^{-4}\ s^{-1}$. Minor ticks on horizontal axis are at 10 min intervals.

the intermediate shown in Scheme 2. The stereochemistry of the donor atoms for the starting six-coordinate complex (*cis*-V) and final five-coordinate complex (*trans*-III) is known from crystallography. Considering the bromide association reaction, as drawn in Scheme 2, the faster step involves N inversion, whereas the slower step is S inversion. The evidence, albeit not definitive, in support of this ordering is that the distinctly different S→Cu charge-transfer transitions in the near-UV region remain after the initial rapid reaction with bromide (Figure 5A), which supports retention of the same S-donor stereochemistry during this first phase. Regardless of the order, we may infer a *trans*-II intermediate in which one amine proton or S-atom lone pair is on the opposite side of the CuN_2S_2 plane from the other lone pairs and amine protons.

Electrochemistry: Reduction of Cu^{II} to Cu^{I} brings a significant change to the coordination geometry preferences of the metal, and the two modes of ligand coordination, tetradentate or hexadentate, will have different abilities to adapt to changes brought about by these redox reactions. Cyclic voltammetry of a solution of [Cu(AMME-N_3S_3sar)Br]Br in DMSO saturated with NaBr to suppress rearrangement (Figure 7A) gave a single reversible one-electron response with cathodic and anodic peaks at −743 and −630 mV

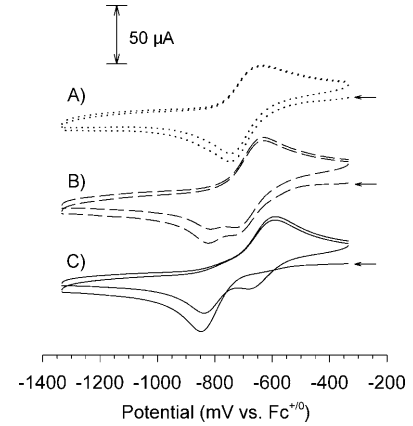

Figure 7. A) Cyclic voltammograms (in DMSO) of 1 mM [Cu(AMME-N_3S_3sar)Br]Br saturated with NaBr, B) 1 mM [Cu(AMME-N_3S_3sar)Br]Br, and C) 1 mM [Cu(AMME-N_3S_3sar)]$(ClO_4)_2$. Experimental conditions: 100 mV s^{-1} sweep rate, glassy carbon working electrode, 0.1 M NEt_4ClO_4 supporting electrolyte. Potentials versus the ferrocene/ferricenium couple. Arrows show direction of initial sweep.

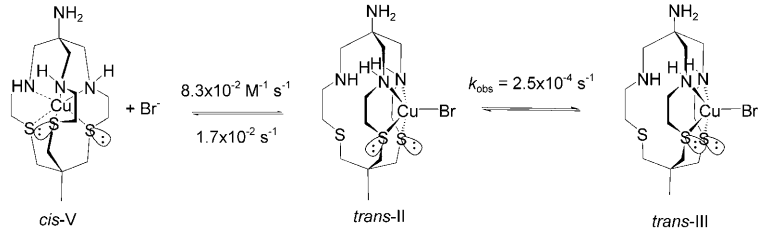

Scheme 2. Rearrangement between hexa- and tetradentate-coordinated Cu^{II} complexes.

versus $Fc^{+/0}$. If NaBr is omitted (Figure 7B), two cathodic waves are apparent at −728 and −825 mV versus $Fc^{+/0}$ but only a single anodic peak on the reverse sweep is seen at −620 mV.

Cyclic voltammetry of the hexadentate-coordinated com-

plex $[Cu(AMME\text{-}N_3S_3sar)]^{2+}$ in DMSO was more complicated (Figure 7C). On the initial cathodic sweep, a single peak was found at −850 mV. On reversal of the sweep, a single anodic peak emerged at a much more positive potential (−600 mV). On successive cycles, a new cathodic peak appeared at −660 mV in addition to the original −850 mV peak. It is clear that the emergent wave coincides with that of five-coordinate $[Cu(AMME\text{-}N_3S_3sar)(OSMe_2)]^{2+}$ (or perhaps with perchlorate coordinated in the axial position). The average peak potential (−630 mV) is significantly higher than that of the bromido complex $[Cu(AMME\text{-}N_3S_3sar)Br]^{+}$ (−687 mV). Remembering that all responses are from complexes confined to the diffusion layer, it is apparent that reduction of six-coordinate $[Cu(AMME\text{-}N_3S_3sar)]^{2+}$ to Cu^{I} results in rapid rearrangement to a tetradentate-coordinated form, thus resembling the five-coordinate complex seen in the crystal structure of $[Cu(AMME\text{-}N_3S_3sar)Br]Br$, but with a solvent coordinated in the axial site in the absence of bromide. This tetradentate-coordinated form then remains in the diffusion layer and reappears in successive cycles. The inherent instability of the six-coordinate Cu^{I} cage complex is not surprising and mirrors the behavior of hexaamine sar analogues in which the confines of the N_6 cage are incommensurate with the preferences of monovalent copper. To date, only the expanded cavity cage complex $[Cu(Me_5tricosane)]^{2+}$ has been found to be capable of stabilizing a monovalent Cu complex,[31] albeit only on the timescale of a cyclic voltammetry experiment and within a narrow window of sweep rates.

Conclusion

The present study shows that despite the typical encapsulating tendency of cage ligands, some remarkable rearrangements can be identified that are triggered by seemingly innocuous ligands such as bromide. Never before has such a major structural transformation been seen in a cage complex without the addition of strong ligands such as cyanide or protonation of the amine donors in strong acid. The results have important consequences for the use of copper complexes of $AMME\text{-}N_3S_3sar$ in metal-catalyzed organic and polymer reactions, as the obligate presence of a bromido ligand is dependent on a number of factors including time, bromide and copper concentration, as well as oxidation state.

Experimental Section

Safety notes: Perchlorate salts are potentially explosive and should be handled in small quantities. These compounds should never be heated in the solid state or scraped from sintered glass frits. Cyanide solutions are potentially lethal. They must always be kept in a well-ventilated fume hood and appropriate personal protective equipment must always be worn when manipulating cyanide solutions. Cyanide waste solutions should be deactivated immediately by oxidation with hypochlorite and should never come into contact with strong acids.

Synthesis: The complex $[Co(\mathbf{H}AMME\text{-}N_3S_3sar)]Cl_4{\cdot}4H_2O$ was prepared as described.[4]

$AMME\text{-}N_3S_3sar{\cdot}0.5H_2O$: A solution of $[Co(\mathbf{H}AMME\text{-}N_3S_3sar)]Cl_4{\cdot}4H_2O$ (11 g; in which the pendent primary amine is protonated) in water (150 mL) was purged with N_2 gas for 15 min. Zn dust (3 g) was added and purging continued for a further 45 min. NaCN (20 g) was added to the resulting purple solution of the Co^{II} complex and the reaction was maintained under an atmosphere of N_2 for 9 d, thereby resulting in a color change to green and the appearance of a colorless precipitate. The solution was made alkaline with KOH solution and the product was extracted with $CHCl_3$ (3×100 mL). The organic layers were collected and dried over anhydrous Na_2SO_4. The solution was filtered and removal of solvent under vacuum gave a pale yellow oil, which solidified to give a semicrystalline slightly yellow solid (7 g, 67%). ^{13}C NMR (D_2O, 1,4-dioxane): δ = 34.67, 40.39, 49.23, 54.91 (-CH_2-), 42.64, 56.91 (C_q), 28.34 ppm (CH_3); ^{13}C NMR ($CDCl_3$, TMS): δ = 35.28, 39.14, 50.07, 53.32 (-CH_2-), 43.82, 61.34 (C_q), 25.03 ppm (CH_3); ^{13}C NMR (DMSO): δ = 35.49, 39.44, 50.48, 54.07 (-CH_2-), 43.61, 62.01 (C_q), 25.64 ppm (CH_3); MS (EI, theoretical): *m*/*z*: 364.18; found: 365.23 $[AMME\text{-}N_3S_3sar]^{+}$; elemental analysis calcd (%) for $C_{15}H_{32}N_4S_3{\cdot}0.5H_2O$: C 48.22, H 8.90, N 14.99, S 25.75%; found: C 48.23, H 8.97, N 14.82, S 25.95.

$[Cu^{II}(AMME\text{-}N_3S_3sar)](ClO_4)_2$: $Cu(NO_3)_2{\cdot}2.5H_2O$ (170 mg, 0.731 mmol) was dissolved in EtOH (1 mL) and added dropwise with constant stirring to a solution of $AMME\text{-}N_3S_3sar$ (250 mg, 0.685 mmol) in EtOH (8 mL) to give an immediately intensely blue solution. After removal of the solvent under vacuum, the complex was redissolved in a solution of sodium perchlorate (0.5 g) in water (6 mL), warmed gently, and filtered. Dark blue octahedral crystals suitable for X-ray analysis formed upon standing; these were filtered off and dried in a vacuum desiccator (307 mg, 49%). Electronic spectrum ([D_6]DMSO): λ_{max} (ε): 1292 (49), 622 (530), 367 (4500), 311 nm (4000 $M^{-1}cm^{-1}$); EPR (DMSO, 140 K, 33.936 GHz): g_z = 2.163 (A_z = 160 G), g_y = 2.076 (A_y = 50 G), and g_x = 2.038 (A_x = 35 G); elemental analysis calcd (%) for $C_{15}H_{32}Cl_2CuN_4O_8S_3$: C 28.72, H 5.14, N 8.93, S 15.34; found: C 28.53, H 5.07, N 8.73, S 15.31.

$[Cu^{II}(AMME\text{-}N_3S_3sar)Br]Br{\cdot}3H_2O$: $AMME\text{-}N_3S_3sar$ (50 mg, 0.14 mmol) was added portionwise over 5 min to a solution of $CuBr_2$ (31 mg, 0.14 mmol) in EtOH (10 mL). The solution turned rapidly from dark brown to dark blue. The solution was filtered and the solvent was removed by rotary evaporation. The solid residue was washed with diethyl ether (2×50 mL). The dark blue solid was redissolved in H_2O (5 mL) and allowed to crystallize by slow evaporation over 3 d. The dark blue-green needles that formed were collected by filtration and dried in a vacuum desiccator (69 mg, 79%). Electronic spectrum (DMSO with 20 mM $n$$Bu_4PBr$): λ_{max} (ε): 641 (770), 336 nm (3660 $M^{-1}cm^{-1}$); EPR (DMSO with 0.1 M Et_4NBr, 140 K, 33.936 GHz): g_z = 2.154 (A_z = 164 G), $g_y = g_x$ = 2.040 ($A_y = A_x$ = 25 G); elemental analysis calcd (%) for $C_{15}H_{32}Br_2CuN_4S_3{\cdot}3H_2O$: C 28.06, H 5.97, N 8.73, S 14.98; found: C 28.12, H 5.45, N 8.59, S 15.19.

Physical methods: Electronic spectra were measured using an Analytik-Jena Specord 2100 spectrophotometer as sample solutions in DMSO or in the presence of bromide ions (as $n$$Bu_4PBr$). Kinetic runs were recorded using Cary50 or HP8453 instruments, equipped with a thermostated multicell holder. All bromido complex association reactions were carried out under pseudo-first-order conditions ($[Br^-]/[Cu^{II}] > 10$) in DMSO as solvent and with the ionic strength kept constant at 0.17 M with $NaClO_4$. The concentrations of the copper complexes were in the range $(1\text{–}5)\times10^{-4}$ M; the general kinetic procedure has been already described.[26] The program Specfit[55] was used for data manipulation and analysis, and observed rate constants were derived from the absorbance versus time traces at wavelengths at which a maximum change in absorbance was observed. Cyclic voltammetry was performed using a BAS100B/W potentiostat employing a glassy carbon working electrode, platinum auxiliary electrode, and nonaqueous $Ag/AgNO_3$ (DMSO) reference electrode that contained 0.1 M Et_4NClO_4 (in DMSO), which was also the supporting electrolyte in all experiments. All solutions contained 1 mM concentrations of copper complex and were purged with nitrogen before measurement. Potentials are cited relative to an external ferricenium/ferrocene ($Fc^{+/0}$) reference potential measured under the same conditions. Electron

paramagnetic resonance (EPR) spectra were measured using a Bruker ER200 instrument at Q-band frequency (≈33 GHz) as 2 mM DMSO frozen solutions at 140 K. In some cases, the solutions also contained Et_4NBr (100 mM) as indicated. Spin Hamiltonian parameters were determined by spectral simulation with the program EPR50F[52] and the simulated spectra are presented in the Supporting Information.

Crystallography: Crystallographic data were collected at 293 K using an Oxford Diffraction Gemini Ultra S CCD diffractometer employing graphite-monochromated $Mo_{K\alpha}$ radiation (0.71073 Å) in the range $2< 2\theta <50°$. Data reduction and empirical absorption corrections were performed using CrysAlisPro (Oxford Diffraction version 171.32.15). Structures were solved by Patterson methods with SHELXS-86 and refined by full-matrix least-squares analysis against F^2 with SHELXL-97[56] within the WinGX package.[57] Alkyl and coordinated amine hydrogen atoms were included at estimated positions, whereas those associated with non-coordinated amines or water molecules were located from difference maps then restrained with a riding model as for alkyl hydrogen atoms. Drawings of molecules were produced using ORTEP3.[58] Crystal data are summarized in Table 1. CCDC-748545 ([Cu(AMME-N_3S_3sar)Br]Br·3H_2O) and 748546 ([Cu(AMME-N_3S_3sar)]$(ClO_4)_2$) contain the supplementary crystallographic data for this paper. These data can be obtained free of charge from The Cambridge Crystallographic Data Centre via www.ccdc.cam.ac.uk/data_request/cif.

Table 1. Crystal data.

	[Cu(AMME-N_3S_3sar)Br]Br·3H_2O	[Cu(AMME-N_3S_3sar)]-$(ClO_4)_2$
dimensions [mm]	0.5×0.1×0.1	0.3×0.2×0.2
crystal system	monoclinic	cubic
space group	$P2_1/n$ (no.14, variant)	$P2_13$ (no.198)
a [Å]	8.157(1)	13.4645(3)
b [Å]	26.235(5)	–
c [Å]	11.835(2)	–
β [°]	107.56(2)	–
V [Å^3]	2414.7(7)	2441.02(9)
ρ_{calcd} [g cm^{-3}]	1.766	1.706
Z	4	4
N_{tot}[a]	12173	2271
N[b] (R_{int})	4205 (0.0264)	1162 (0.0299)
N_o[c] ($I>2\sigma(I)$)	2915	828
R_1 (obsd data)	0.0296	0.0448
wR_2 (all data)	0.0570	0.1062

[a] Number of reflections measured. [b] Number of unique reflections. [c] Number of observed reflections.

Acknowledgements

P.V.B., M.J.M., and L.R.G. wish to acknowledge the Australian Research Council for grant support, and M.M. acknowledges DGI grant CTQ2009-14443-C02-02. We also wish to thank Dr. Chris Noble (Centre for Magnetic Resonance, University of Queensland) for assistance with the EPR measurements.

[1] I. I. Creaser, J. M. Harrowfield, A. J. Herlt, A. M. Sargeson, J. Springborg, R. J. Geue, M. R. Snow, *J. Am. Chem. Soc.* **1977**, *99*, 3181.
[2] R. J. Geue, T. W. Hambley, J. M. Harrowfield, A. M. Sargeson, M. R. Snow, *J. Am. Chem. Soc.* **1984**, *106*, 5478.
[3] P. Osvath, A. M. Sargeson, B. W. Skelton, A. H. White, *J. Chem. Soc. Chem. Commun.* **1991**, 1036.
[4] L. R. Gahan, T. W. Hambley, A. M. Sargeson, M. R. Snow, *Inorg. Chem.* **1982**, *21*, 2699.
[5] R. V. Dubs, L. R. Gahan, A. M. Sargeson, *Inorg. Chem.* **1983**, *22*, 2523.
[6] P. A. Lay, J. Lydon, A. W. H. Mau, P. Osvath, A. M. Sargeson, W. H. F. Sasse, *Aust. J. Chem.* **1993**, *46*, 641.
[7] P. Osvath, A. M. Sargeson, A. McAuley, R. E. Mendelez, S. Subramanian, M. J. Zaworotko, L. Broge, *Inorg. Chem.* **1999**, *38*, 3634.
[8] T. M. Donlevy, L. R. Gahan, T. W. Hambley, R. Stranger, *Inorg. Chem.* **1992**, *31*, 4376.
[9] T. M. Donlevy, L. R. Gahan, R. Stranger, S. E. Kennedy, K. A. Byriel, C. H. L. Kennard, *Inorg. Chem.* **1993**, *32*, 6023.
[10] T. M. Donlevy, L. R. Gahan, T. W. Hambley, *Inorg. Chem.* **1994**, *33*, 2668.
[11] T. M. Donlevy, T. W. Hambley, G. R. Hanson, K. L. McMahon, R. Stranger, L. R. Gahan, *Inorg. Chem.* **1994**, *33*, 5131.
[12] J. I. Bruce, L. R. Gahan, T. W. Hambley, R. Stranger, *Inorg. Chem.* **1993**, *32*, 5997.
[13] J. I. Bruce, L. R. Gahan, T. W. Hambley, R. Stranger, *J. Chem. Soc. Chem. Commun.* **1993**, 702.
[14] P. A. Lay, A. Mau, W. H. F. Sasse, I. I. Creaser, L. R. Gahan, A. M. Sargeson, *Inorg. Chem.* **1983**, *22*, 2347.
[15] L. R. Gahan, G. A. Lawrance, A. M. Sargeson, *Inorg. Chem.* **1984**, *23*, 4369.
[16] L. R. Gahan, T. M. Donlevy, T. W. Hambley, *Inorg. Chem.* **1990**, *29*, 1451.
[17] C. A. Sharrad, L. R. Gahan, *Polyhedron* **2003**, *22*, 45.
[18] C. A. Sharrad, L. Grondahl, L. R. Gahan, *J. Chem. Soc. Dalton Trans.* **2001**, 2937.
[19] P. V. Bernhardt, J. M. Harrowfield, D. C. R. Hockless, A. M. Sargeson, *Inorg. Chem.* **1994**, *33*, 5659.
[20] J. R. Roeper, H. Elias, *Inorg. Chem.* **1992**, *31*, 1202.
[21] H. Elias, R. Schumacher, J. Schwamberger, T. Wittekopf, L. Helm, A. E. Merbach, S. Ulrich, *Inorg. Chem.* **2000**, *39*, 1721.
[22] C. Bucher, E. Duval, J.-M. Barbe, J.-N. Verpeaux, C. Amatore, R. Guilard, L. Le Pape, J.-M. Latour, S. Dahaoui, C. Lecomte, *Inorg. Chem.* **2001**, *40*, 5722.
[23] M. S. Seo, J. Y. Kim, J. Annaraj, Y. Kim, Y.-M. Lee, S.-J. Kim, J. Kim, W. Nam, *Angew. Chem.* **2007**, *119*, 381; *Angew. Chem. Int. Ed.* **2007**, *46*, 377.
[24] S. N. Dhuri, M. S. Seo, Y.-M. Lee, H. Hirao, Y. Wang, W. Nam, S. Shaik, *Angew. Chem.* **2008**, *120*, 3404; *Angew. Chem. Int. Ed.* **2008**, *47*, 3356.
[25] G. A. Bottomley, I. J. Clark, I. I. Creaser, L. M. Engelhardt, R. J. Geue, K. S. Hagen, J. M. Harrowfield, G. A. Lawrance, P. A. Lay, A. M. Sargeson, A. J. See, B. W. Skelton, A. H. White, F. R. Wilner, *Aust. J. Chem.* **1994**, *47*, 143.
[26] G. Aullón, P. V. Bernhardt, F. Bozoglian, M. Font-Bardia, B. P. Macpherson, M. Martinez, C. Rodriguez, X. Solans, *Inorg. Chem.* **2006**, *45*, 8551.
[27] M. G. Basallote, P. V. Bernhardt, T. Calvet, C. E. Castillo, M. Font-Bardía, M. Martínez, C. Rodríguez, *Dalton Trans.* **2009**, 9567.
[28] M. A. Halcrow, *Dalton Trans.* **2003**, 4375.
[29] B. Murphy, B. Hathaway, *Coord. Chem. Rev.* **2003**, *243*, 237.
[30] P. V. Bernhardt, R. Bramley, L. M. Engelhardt, J. M. Harrowfield, D. C. R. Hockless, B. R. Korybut-Daszkiewicz, E. R. Krausz, T. Morgan, A. M. Sargeson, B. W. Skelton, A. H. White, *Inorg. Chem.* **1995**, *34*, 3589.
[31] P. V. Bernhardt, R. Bramley, R. J. Geue, S. F. Ralph, A. M. Sargeson, *Dalton Trans.* **2007**, 1244.
[32] L. Grondahl, PhD Thesis, University of Copenhagen (Copenhagen), **1994**.
[33] L. Grondahl, A. Hammershoi, A. M. Sargeson, V. J. Thoem, *Inorg. Chem.* **1997**, *36*, 5396.
[34] A. G. Algarra, M. G. Basallote, C. E. Castillo, M. P. Clares, A. Ferrer, E. García-España, J. M. Llinares, M. A. Máñez, *Inorg. Chem.* **2009**, *48*, 902.
[35] J. Kotek, P. Lubal, P. Hermann, I. Cisarova, I. Lukes, T. Godula, I. Svobodová, P. Táborsky, J. Havel, *Chem. Eur. J.* **2003**, *9*, 233.

[36] I. I. Creaser, J. M. Harrowfield, G. A. Lawrance, W. Mulac, D. Sangster, A. M. Sargeson, K. Schmidt, J. C. Sullivan, *J. Coord. Chem.* **1991**, *23*, 389.
[37] V. Percec, T. Guliashvili, J. S. Ladislaw, A. Wistrand, A. Stjerndahl, M. J. Sienkowska, M. J. Monteiro, S. Sahoo, *J. Am. Chem. Soc.* **2006**, *128*, 14156.
[38] V. Percec, A. V. Popov, E. Ramirez-Castillo, M. Monteiro, B. Barboiu, O. Weichold, A. D. Asandei, C. M. Mitchell, *J. Am. Chem. Soc.* **2002**, *124*, 4940.
[39] K. Matyjaszewski, J. Xia, *Chem. Rev.* **2001**, *101*, 2921.
[40] T. Pintauer, K. Matyjaszewski, *Chem. Soc. Rev.* **2008**, *37*, 1087.
[41] C. A. Bell, M. R. Whittaker, L. R. Gahan, M. J. Monteiro, *J. Polym. Sci. Part A* **2008**, *46*, 146.
[42] N. V. Tsarevsky, K. Matyjaszewski, *Chem. Rev.* **2007**, *107*, 2270.
[43] B. Bosnich, C. K. Poon, M. L. Tobe, *Inorg. Chem.* **1965**, *4*, 1102.
[44] P. Comba, G. A. Lawrance, M. Rossignoli, B. W. Skelton, A. H. White, *Aust. J. Chem.* **1988**, *41*, 773.
[45] G. Wei, C. C. Allen, T. W. Hambley, G. A. Lawrance, M. Maeder, *Aust. J. Chem.* **1995**, *48*, 825.
[46] B. J. Hathaway, *Struct. Bonding (Berlin)* **1984**, *57*, 55.
[47] D. L. Cullen, E. C. Lingafelter, *Inorg. Chem.* **1970**, *9*, 1858.
[48] J. Ammeter, H. B. Buergi, E. Gamp, V. Meyer-Sandrin, W. P. Jensen, *Inorg. Chem.* **1979**, *18*, 733.
[49] P. Comba, *Inorg. Chem.* **1989**, *28*, 426.
[50] P. E. M. Wijnands, J. S. Wood, J. Reedijk, W. J. A. Maaskant, *Inorg. Chem.* **1996**, *35*, 1214.
[51] P. Chaudhuri, K. Oder, K. Wieghardt, J. Weiss, J. Reedijk, W. Hinrichs, J. Wood, A. Ozarowski, H. Stratemaier, D. Reinen, *Inorg. Chem.* **1986**, *25*, 2951.
[52] R. A. Martinelli, G. R. Hanson, J. S. Thompson, B. Holmquist, J. R. Pilbrow, D. S. Auld, B. L. Vallee, *Biochemistry* **1989**, *28*, 2251.
[53] Y. Ducommun, A. E. Merbach in *Inorganic High Pressure Chemistry*, Elsevier, Amsterdam, **1986**, pp. 69.
[54] W. G. Jackson, A. M. Sargeson, *Inorg. Chem.* **1978**, *17*, 2165.
[55] SPECFIT. Global analysis system, R. A. Binstead, Spectrum Software Associates, Marlborough, **2007**.
[56] SHELX Release 97-2 ed., G. M. Sheldrick, University of Göttingen, Göttingen, **1997**.
[57] L. J. Farrugia, *J. Appl. Crystallogr.* **1999**, *32*, 837.
[58] L. J. Farrugia, *J. Appl. Crystallogr.* **1997**, *30*, 565.

Received: September 23, 2009
Published online: February 4, 2010

